Ternary Arsenide $Ba_{0.8}Hf_{12}As_{17.7}$, a Variant of the $Cr_{12}P_7$ Structure Type with Inserted Arsenic Ribbons

Robert Lam and Arthur Mar*

Department of Chemistry, University of Alberta, Edmonton, Alberta, Canada T6G 2G2

Received May 14, 1998

The nonstoichiometric ternary barium hafnium arsenide $Ba_{0.8}Hf_{12}As_{17.7}$ has been synthesized through reaction of the elements at 950 °C in a tin flux, and its structure has been determined by single-crystal X-ray diffraction methods. It crystallizes in the hexagonal space group C_{6h}^2-$P6_3/m$ with $a = 14.997(1)$ Å, $c = 3.5526(4)$ Å, and $Z = 1$ at 22 °C. The structure consists of columns of As-centered Hf_6 trigonal prisms aligned along [001]. It is derived from the $Cr_{12}P_7$ structure type (the anti-type of Th_7S_{12}) by inserting six-atom wide As ribbons between assemblies of the trigonal prismatic columns. Alternatively, $Ba_{0.8}Hf_{12}As_{17.7}$ may be considered to be an antitype of the $Ho_6Ni_{20}P_{13}$ structure type but with nonmetal homoatomic bonding being a predominant feature. The weakly metallic behavior and some of the features of As−As bonding in $Ba_{0.8}Hf_{12}As_{17.7}$ are supported by extended Hückel band structure calculations.

Introduction

Ternary pnictides of the early transition metals provide fertile ground for discovering new classes of Zintl compounds.[1] The transition metal component introduces the potential for d electrons to participate in a variety of interesting electrical and magnetic phenomena, such as colossal magnetoresistance in $Eu_{14}MnSb_{11}$.[2] The restriction to the early transition metals rests on the expectation that phases isostructural to the main group analogues can be prepared. Thus, for instance, the $A_{14}MnPn_{11}$ (A = Ca, Sr, Ba, Eu; Pn = P, As, Sb, Bi) phases[1−4] adopt the $Ca_{14}AlSb_{11}$ structure type.[5] There are few other ternary alkaline earth arsenides of the early transition metals known (A_4TiPn_4 (A = Sr, Ba; Pn = P, As),[6] quaternary Na_5SrMP_4 (M = Nb, Ta),[7] and ACr_2As_2 (A = Ca, Sr, Ba)[8]), none of these exhibiting As−As bonding.

We report here the synthesis and structure of the nonstoichiometric ternary arsenide $Ba_{0.8}Hf_{12}As_{17.7}$. While an analogous main group compound is not expected (because of the high CN of Hf), $Ba_{0.8}Hf_{12}As_{17.7}$ displays the unusual feature of As ribbons inserted between isolated columnar assemblies of Hf_6 trigonal prisms. These ribbons represent, to our knowledge, the first example of the stabilization of extended homoatomic bonding of the nonmetal (or metalloid) component within the large family of hexagonal structures based on the stacking of trigonal prisms.[9] Extended Hückel band structure calculations are presented to lend insight into the nature of As−As bonding in $Ba_{0.8}Hf_{12}As_{17.7}$.

Experimental Section

Synthesis. Single crystals of $Ba_{0.8}Hf_{12}As_{17.7}$ were obtained from reaction of a 0.25-g mixture of Ba, Hf, and As in a 3:1:5 ratio in a tin flux (Ba, 107 mg, 0.78 mmol, 99.9%, Alfa-Aesar; Hf, 46 mg, 0.26 mmol, 99.8%, Cerac; As, 97 mg, 1.30 mmol, 99.99%, Alfa-Aesar; Sn, 309 mg, 2.60 mmol, 99.8%, Cerac) loaded into a sealed and evacuated fused-silica tube (7 cm length, 10 mm i.d.). The mixture was heated at 600 °C for 1 day and 950 °C for 2 days, cooled to 600 °C over 1 day, and then cooled to room temperature over 10 h. Dissolving the excess Sn in concentrated HCl afforded thin needles of the ternary compound, as well as the binary phases HfAs[10] and Sn_4As_3[11] as byproducts. EDX (energy-dispersive X-ray) analysis of these crystals on a Hitachi F2700 scanning electron microscope confirmed the presence of all three elements (Ba, 3(1); Hf, 44(1); As, 53(1) mol %; average of 8 analyses) and the absence of any residual Sn. The observed powder X-ray diffraction pattern of $Ba_{0.8}Hf_{12}As_{17.7}$, obtained on an Enraf-Nonius FR552 Guinier camera (Cu $K\alpha_1$ radiation; Si standard), agrees well with that calculated from the crystal structure by the program LAZY-PULVERIX[12] (Table S1).

Structure Determination. Weissenberg photographs clearly revealed Laue symmetry 6/m and gave preliminary cell parameters. Final cell parameters were determined from a least-squares analysis of the setting angles of 38 reflections in the range $18° \le 2\theta(\text{Mo K}\alpha) \le 29°$ centered on a Siemens P4RA diffractometer. Crystal data and further details of the data collection are given in Table 1 and the CIF (Supporting Information).

Calculations were carried out with the use of programs in the SHELXTL (version 5.0) package.[13] Conventional atomic scattering

(1) Kauzlarich, S. M., Ed. *Chemistry, Structure, and Bonding of Zintl Phases and Ions*; VCH Publishers: New York, 1996.
(2) Chan, J. Y.; Kauzlarich, S. M.; Klavins, P.; Shelton, R. N.; Webb, D. J. *Chem. Mater.* **1997**, *9*, 3132.
(3) Rehr, A.; Kuromoto, T. Y.; Kauzlarich, S. M.; Del Castillo, J.; Webb, D. J. *Chem. Mater.* **1994**, *6*, 93.
(4) Chan, J. Y.; Wang, M. E.; Rehr, A.; Kauzlarich, S. M.; Webb, D. J. *Chem. Mater.* **1997**, *9*, 2131 (and references therein).
(5) Cordier, G.; Schäfer, H.; Stelter, M. *Z. Anorg. Allg. Chem.* **1984**, *519*, 183.
(6) Nuss, J.; Hönle, W.; Peters, K.; von Schnering, H. G. *Z. Anorg. Allg. Chem.* **1996**, *622*, 1879.
(7) Lin, J.; Hönle, W.; von Schnering, H. G. *J. Alloys Compd.* **1992**, *183*, 403.
(8) Pfisterer, M.; Nagorsen, G. *Z. Naturforsch., B: Anorg. Chem., Org. Chem.* **1980**, *35*, 703.
(9) Pivan, J.-Y.; Guérin, R.; Sergent, M. *J. Solid State Chem.* **1987**, *68*, 11.
(10) Jeitschko, W.; Nowotny, H. *Monatsh. Chem.* **1962**, *93*, 1284.
(11) Eckerlin, P.; Kischio, W. *Z. Anorg. Allg. Chem.* **1968**, *363*, 1.
(12) Yvon, K.; Jeitschko, W.; Parthé, E. *J. Appl. Crystallogr.* **1977**, *10*, 73.
(13) Sheldrick, G. M. *SHELXTL* version 5.0; Siemens Analytical X-ray Instruments, Inc.: Madison, WI, 1994.

S0020-1669(98)00545-X CCC: $15.00
Published on Web 09/15/1998

Table 1. Crystallographic Data for $Ba_{0.8}Hf_{12}As_{17.7}$

$Ba_{0.8}Hf_{12}As_{17.7}$	$T = 22$ °C
fw 3577.85	$\lambda = 0.710\ 73$ Å
$a = 14.997(1)$ Å[a]	$\rho_{calcd} = 8.617$ g cm^{-3}
$c = 3.5526(4)$ Å[a]	μ(Mo Kα) = 670.6 cm^{-1}
$V = 692.0(1)$ Å^3 [a]	$R(F)$ for $F_o^2 > 2((F_o^2)^b = 0.063$
$Z = 1$	$R_w(F_o^2)^c = 0.118$
C_{6h}^2-$P6_3/m$ (No. 176)	

[a] Obtained from a refinement constrained so that $\alpha = \beta = 90°$ and $\gamma = 120°$. [b] $R(F) = \sum||F_o| - |F_c||/\sum|F_o|$. [c] $R_w(F_o^2) = [\sum[w(F_o^2 - F_c^2)^2]/\sum wF_o^4]^{1/2}$; $w^{-1} = [\sigma^2(F_o^2) + (0.0356p)^2 + 0.00p]$, where $p = [\max(F_o^2,0) + 2F_c^2]/3$.

Table 2. Atomic Coordinates and Equivalent Isotropic Displacement Parameters (Å^2) for $Ba_{0.8}Hf_{12}As_{17.7}$

atom	Wyckoff position	x	y	z	U_{eq}[a]
Ba[b]	4e	0	0	0.137(3)	0.033(6)
Hf(1)	6h	0.35495(7)	0.11892(7)	$^1/_4$	0.0042(2)
Hf(2)	6h	0.61802(8)	0.17720(8)	$^1/_4$	0.0042(2)
As(1)[b]	6h	0.0142(3)	0.4500(3)	$^1/_4$	0.006(1)
As(2)	6h	0.0718(2)	0.2384(2)	$^1/_4$	0.0053(5)
As(3)	6h	0.2850(2)	0.5099(2)	$^1/_4$	0.0027(4)
As(4)[b]	6h	0.3422(5)	0.2965(5)	$^1/_4$	0.007(2)

[a] U_{eq} is defined as one-third of the trace of the orthogonalized $\mathbf{U}_{ij}$ tensor. [b] Occupancies are 20.9(6)% for Ba, 56(1)% for As(1), and 39(1)% for As(4).

factors and anomalous dispersion corrections were used.[14] Intensity data were processed, and face-indexed Gaussian-type absorption corrections were applied in XPREP. The systematic extinction (00l: $l = 2n + 1$) was noted, suggesting C_6^6-$P6_3$ and C_{6h}^2-$P6_3/m$ as possible space groups. The centrosymmetric space group $P6_3/m$ was chosen on the basis of intensity statistics, satisfactory averaging, and the successful structure solution. The initial positions of the Hf and As atoms were found by direct methods, and the structure was refined by least-squares methods. Residual electron density at 0, 0, ~0.14 was assigned to Ba on the basis of reasonable Ba−As distances. Note, however, that full occupation of Ba atoms at this site results in close contacts (<1 Å) between symmetry-equivalent positions, as well as a very high value for the displacement parameter. The As(1) and As(4) sites also revealed anomalously large displacement parameters. When the occupancy parameters for these sites were refined, they converged to values of 20.9(6)% for Ba, 56(1)% for As(1), and 39(1)% for As(4), and the displacement parameters were now comparable to those of the other atoms. The occupancies of the Hf(1), Hf(2), As(2), and As(3) atoms were essentially 100%. The resulting formula, $Ba_{0.8}Hf_{12}As_{17.7}$, is consistent with the chemical analysis determined independently (vide supra). The atomic positions were standardized with the use of the program STRUCTURE TIDY.[15] The final cycle of least-squares refinement on F_o^2 of 44 variables (including anisotropic displacement parameters and an isotropic extinction parameter) and 1148 averaged reflections (including those having $F_o^2 < 0$) converged to values of $R_w(F_o^2)$ of 0.118 and $R(F)$ (for $F_o^2 > 2((F_o^2))$ of 0.063. The final difference electron density map is featureless ($\Delta\rho_{max} = 5.58$; $\Delta\rho_{min} = -5.36$ e Å^{-3}). Final values of the positional and equivalent isotropic displacement parameters are given in Table 2, anisotropic displacement parameters are in the CIF, and final structure amplitudes are available from A.M.

Electrical Resistivity. Single crystals of ~0.5 mm length, verified to be $Ba_{0.8}Hf_{12}As_{17.7}$ by EDX analysis, were mounted with Ag paint on Au wires with graphite extensions. Four-probe ac electrical resistivity data were measured along the needle axis c of these crystals between 25 and 290 K.

Band Structure. One-electron band structure calculations on the hypothetical fully stoichiometric $[Hf_{12}As_{24}]$ substructure were performed by the tight-binding method with an extended Hückel-type Hamiltonian.[16,17] Extended Hückel parameters used[18,19] are listed in Table 3. Properties were extracted from the band structure using 50 k points in the irreducible portion of the Brillouin zone.[20]

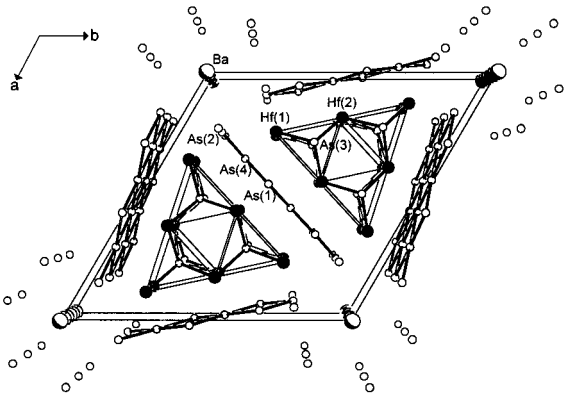

Figure 1. View of $Ba_{0.8}Hf_{12}As_{17.7}$ down the c axis with the unit cell outlined and the atoms labeled. The large partly shaded circles are Ba atoms, the medium solid circles are Hf atoms, and the small open circles are As atoms.

Table 3. Extended Hückel Parameters[18,19]

atom	orbital	H_{ii} (eV)	ζ_1	c_1	ζ_2	c_2
Hf	6s	−8.12	2.21			
	6p	−4.50	2.17			
	5d	−8.14	4.36	0.6967	1.709	0.5322
As	4s	−16.22	2.23			
	4p	−12.16	1.89			

Table 4. Selected Interatomic Distances (Å) and Angles (deg) for $Ba_{0.8}Hf_{12}As_{17.7}$

Ba−As(2)	3.202(3) (×3)	Hf(2)−As(3)	2.730(2) (×2)
Ba−As(2)	3.461(5) (×3)	Hf(2)−As(3)	2.740(2) (×2)
Ba−As(2)	3.852(7) (×3)	Hf(2)−As(1)	2.794(3) (×2)
Hf(1)−As(3)	2.718(2) (×2)	Hf(2)−As(1)	2.805(4)
Hf(1)−As(4)	2.763(7)	Hf(2)−As(4)	2.839(7)
Hf(1)−As(4)	2.803(5) (×2)	As(1)−As(1)	2.495(6) (×2)
Hf(1)−As(1)	2.806(4)	As(1)−As(4)	2.599(5) (×2)
Hf(1)−As(2)	2.823(2) (×2)	As(2)−As(4)	2.518(5) (×2)
Hf(1)−As(2)	2.842(3)		

As(2)−Ba−As(2)	118.45(9) (×3)	As(4)−As(1)−As(4)	86.2(2)
As(2)−Ba−As(2)	163.8(4) (×3)	As(4)−As(2)−As(4)	89.7(2)
As(2)−Ba-As(2)	105.3(2) (×3)	As(2)−As(4)−As(2)	89.7(2)
As(2)−Ba−As(2)	66.08(4) (×6)	As(2)−As(4)−As(1)	92.01(8) (×2)
As(1)−As(1)−As(1)	90.8(3)	As(1)−As(4)−As(1)	86.2(2)
As(1)−As(1)−As(4)	91.5(1) (×2)		

Results and Discussion

Description of the Structure. $Ba_{0.8}Hf_{12}As_{17.7}$ adopts a novel structure, shown in a projection down the short c axis in Figure 1. Selected interatomic distances and angles are listed in Table 4. To draw structural relationships, it will be advantageous to view the structure of $Ba_{0.8}Hf_{12}As_{17.7}$ as comprising assemblies of As(3)-centered trigonal prisms whose vertexes are the Hf(1) and Hf(2) atoms. Three $AsHf_6$ trigonal prisms are linked to give a larger triangular grouping, in turn generating a vacant site at $^1/_3$, $^2/_3$, $^1/_4$. The triangular faces of these trigonal prisms are then shared to give the columnar assemblies $^1_\infty[As_3Hf_6]$

(14) *International Tables for X-ray Crystallography*; Wilson, A. J. C., Ed.; Kluwer: Dordrecht, The Netherlands, 1992; Vol. C.
(15) Gelato, L. M.; Parthé, E. *J. Appl. Crystallogr.* **1987**, *20*, 139.
(16) Whangbo, M.-H.; Hoffmann, R. *J. Am. Chem. Soc.* **1978**, *100*, 6093.
(17) Hoffmann, R. *Solids and Surfaces: A Chemist's View of Bonding in Extended Structures*; VCH Publishers: New York, 1988.
(18) Kleinke, H.; Franzen, H. F. *J. Alloys Compd.* **1997**, *225*, 110.
(19) Johrendt, D.; Mewis, A. *Z. Naturforsch., B: Chem. Sci.* **1996**, *51*, 655.
(20) Ramírez, R.; Böhm, M. C. *Int. J. Quantum Chem.* **1986**, *30*, 391.

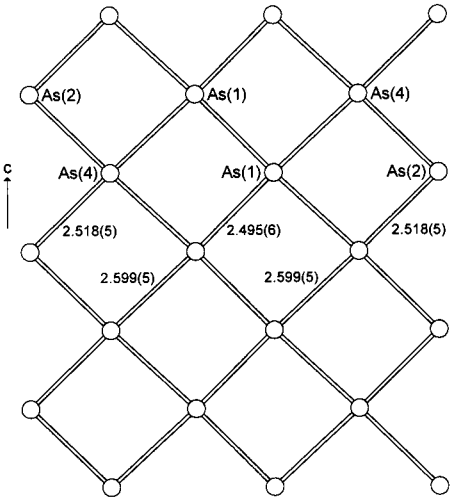

Figure 2. View of the As ribbon in $Ba_{0.8}Hf_{12}As_{17.7}$ running along *c* and built up from As(2), As(4), and As(1).

running along [001]. Separating these columns are Ba cations and six-atom wide ribbons built up from As(1), As(2), and As(4). Figure 2 shows a view perpendicular to one of these As ribbons, which consists of alternating short (As(2)−As(4) 2.518(5) Å, As(1)−As(1) 2.495(6) Å) and long (As(1)−As(4) 2.599(5) Å) bonds. These distances are slightly longer than those for typical As−As single bonds (2.4−2.5 Å).[21−26] The ribbons are nearly flat, with As−As−As bond angles of 86.2(2)−92.01(8)°. While the As(2) sites at the two edges of the ribbon are fully occupied, the inner As(1) and As(4) sites are deficient, with occupancies of 56(1)% and 39(1)%, respectively. These ribbons may be considered to be excised from infinite square nets, which form a common motif in the structures of many pnictides and chalcogenides.[27] In particular, square nets of partially occupied (57.5%) As sites, at comparable As−As distances of 2.563(7) Å, also occur in the compound $Zr_2As_{1.9}S$ (ZrSiS-type structure).[28] One interpretation for the As vacancies is that the ribbon is constructed locally from finite zigzag segments of As atoms, stitched together at irregular intervals. We have not detected any superstructure reflections that might suggest long-range order of these As vacancies.

Alternatively, the more conventional approach of viewing the structure as consisting of coordination polyhedra centered by the electropositive Hf and Ba atoms is also useful. The Hf atoms adopt two types of coordination geometries, as shown in Figure 3. The Hf(1) atoms are coordinated by nine As atoms at distances of 2.718(2)−2.842(3) Å in a monocapped square antiprism, the capping As atom being tilted to one side as is characteristically observed. The Hf(2) atoms are coordinated by eight As atoms at distances of 2.730(2)−2.839(7) Å in a more regular square antiprism. These Hf−As distances are comparable to those in the binary $HfAs_2$ (2.77(5)−2.92(2) Å),

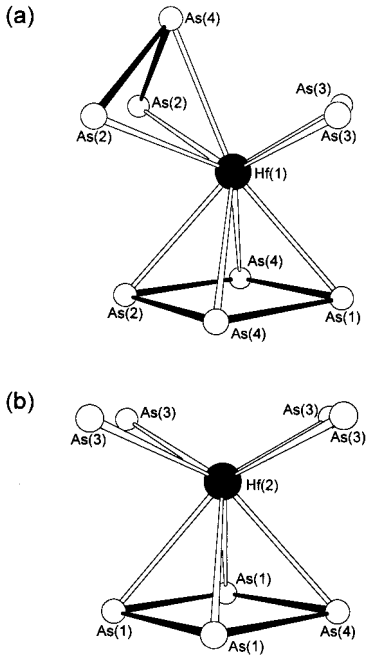

Figure 3. Coordination environment around (a) monocapped square antiprismatic Hf(1) and (b) square antiprismatic Hf(2) in $Ba_{0.8}Hf_{12}As_{17.7}$.

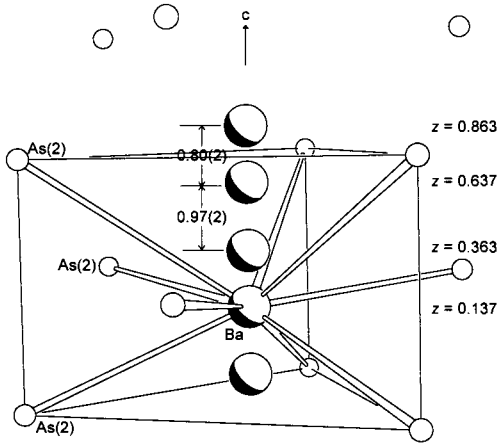

Figure 4. Coordination environment around the Ba atom (at 0, 0, 0.137) in $Ba_{0.8}Hf_{12}As_{17.7}$, disordered among symmetry-equivalent sites along the 6-fold axis (0, 0, *z* at the *z* coordinates shown).

in which a similar Hf monocapped square antiprismatic coordination is found.[10] The Ba atoms, at the sites 4e (0, 0, *z*, with $z = 0.137$), are located along the 6-fold axes within channels outlined by the As(2) atoms. Each Ba atom is coordinated by nine As(2) atoms at distances of 3.202(3)−3.852(7) Å in a tricapped trigonal prism. As shown in Figure 4, the short 0.80(2) and 0.97(2) Å contacts preclude full occupancy of these sites. The refined partial occupancy of 20.9(6)% implies that approximately every fourth site contains a Ba atom, consistent with a reasonable minimum Ba−Ba separation equal to the *c* repeat (3.5526(4) Å). Perhaps the best interpretation of this disorder is that first proposed for the closely related $V_{12}P_7$ structure:[29] while there may be local ordering of Ba atoms along a particular 6-fold axis (i.e., only one of the four possible sites 0, 0, 0.137; 0, 0, 0.363; 0, 0, 0.637; or 0, 0, 0.863 is occupied), it is the distribution of such axes that is either random or incommensurate with the unit cell repeats.

(21) Somer, M.; Carillo-Cabrera, W.; Peters, K.; von Schnering, H. G. *Z. Kristallogr.* **1995**, *210*, 876.
(22) Hönle, W.; Lin, J.; Hartweg, M.; von Schnering, H. G. *J. Solid State Chem.* **1992**, *97*, 1.
(23) Bauhofer, W.; Wittmann, M.; von Schnering, H. G. *J. Phys. Chem. Solids* **1981**, *42*, 687.
(24) Deller, K.; Eisenmann, B. *Z. Naturforsch., B: Anorg. Chem., Org. Chem.* **1977**, *32*, 1368.
(25) Iandelli, A.; Franceschi, E. *J. Less-Common Met.* **1973**, *30*, 211.
(26) Schmettow, W.; von Schnering, H. G. *Angew. Chem., Int. Ed. Engl.* **1977**, *16*, 857.
(27) Tremel, W.; Hoffmann, R. *J. Am. Chem. Soc.* **1987**, *109*, 124.
(28) Barthelat, J. C.; Jeannin, Y. *J. Less-Common Met.* **1972**, *26*, 273.
(29) $V_{12}P_7$: Olofsson, O.; Ganglberger, E. *Acta Chem. Scand.* **1970**, *24*, 2389.

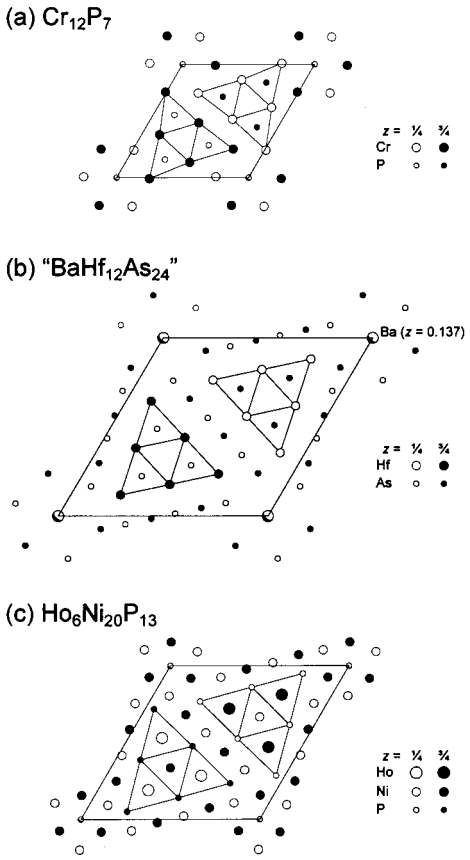

Figure 5. Comparison of the structures of (a) $Cr_{12}P_7$,[30] (b) "$BaHf_{12}As_{24}$" (idealized formula), and (c) $Ho_6Ni_{20}P_{13}$,[34] shown in projection down the hexagonal *c* axis.

Structural Relationships. The formula of the title compound may be represented as $Ba_{1-x}Hf_{12}As_{24-y}$, where there are deficiencies in both the Ba and As sites. Assuming exactly 25% occupancy of the Ba site (necessary to maintain sensible Ba−Ba separations) and 100% occupancy of all As sites, we will refer to the ideal formula as $BaHf_{12}As_{24}$ for the discussion that follows. This helps to draw attention to its close relation to a large family of hexagonal structure types with a metal/nonmetal ratio close to 2 and built up of linked trigonal prisms.[9] However, there are some unique differences displayed by $BaHf_{12}As_{24}$ that make it a novel addition to this family. $BaHf_{12}As_{24}$ is best regarded as an intermediate structure type between the $Cr_{12}P_7$ (*anti*-Th_7S_{12})[29−33] and $Ho_6Ni_{20}P_{13}$ types,[34−38] as shown in Figure 5. All three structures share the feature of the large triangular assembly of linked trigonal prisms extended as columns along the 3-fold axes of the unit cell. From one point of view, $Cr_{12}P_7$ and $BaHf_{12}As_{24}$ are similar in having the nonmetal atoms centered in the outermost trigonal prisms whose vertexes are the metal atoms; the central trigonal prism remains vacant. Then, insertion of ribbons of As atoms into tetrahedral (As(1), As(4)) and trigonal pyramidal (As(2)) sites between these triangular assemblies results in the $BaHf_{12}As_{24}$ structure. From another point of view, $BaHf_{12}As_{24}$ can be regarded as an antitype of the $Ho_6Ni_{20}P_{13}$ structure, in which the metal and nonmetal atoms are interchanged. Moreover, there is a triangular (planar) site at $^1/_3$, $^2/_3$, $^1/_4$ that is occupied by a Ni atom in $Ho_6Ni_{20}P_{13}$ but is vacant in $BaHf_{12}As_{24}$. The Ni atom closest to the 6-fold axis is disordered over two closely spaced sites in $Ho_6Ni_{20}P_{13}$,[34] while the corresponding As atom is well-behaved in $BaHf_{12}As_{24}$. This occurs in association with the disorder of the atom occupying the channels along the 6-fold axis 0, 0, *z*. While it is at $z = 0$ or $z = ^1/_4$ where a small nonmetal atom is located for most $Cr_{12}P_7$- and $Ho_6Ni_{20}P_{13}$-related structures, the large Ba atom achieves its high CN to surrounding As atoms by being situated at $z = 0.137$. The relationship among the $Cr_{12}P_7$, $BaHf_{12}As_{24}$, and $Ho_6Ni_{20}P_{13}$ structures is summarized in Table 5, which shows the correspondence between the various atomic sites and their occupation.

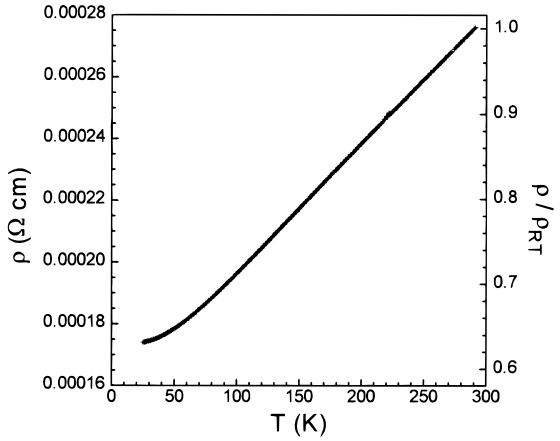

Figure 6. Plot of the electrical resistivity of $Ba_{0.8}Hf_{12}As_{17.7}$, measured along the needle axis *c*.

Table 5. Comparison of Site Occupation[29−38]

sites	$Cr_{12}P_7$	$BaHf_{12}As_{24}$[a]	$Ho_6Ni_{20}P_{13}$
trigonal prisms	6 P	6 As	6 Ho
tetrahedra and pyramids		18 As	18 Ni
triangles			2 Ni
vertices of trigonal prisms	12 Cr	12 Hf	12 P
disordered sites along 0, 0, *z*	1 P	1 Ba	1 P

[a] Ideal formula assuming 25% Ba and 100% As occupancies.

Electrical Resistivity. A representative plot of the electrical resistivity of $Ba_{0.8}Hf_{12}As_{17.7}$, measured along the needle axis *c*, as a function of temperature, is shown in Figure 6. It is poorly metallic with resistivity values ($\rho_{290} \approx 3 \times 10^{-4}$ Ω cm, $\rho_{25} \approx 2 \times 10^{-4}$ Ω cm, and $\rho_{290}/\rho_{25} \approx 0.63$) that are consistent among several samples. For the linear portion of the curve, the temperature coefficient is 4×10^{-7} Ω cm K^{-1}. The plateau at low-temperature arises from impurity scattering.

Bonding. Whether one considers the idealized formula $BaHf_{12}As_{24}$ or the observed nonstoichiometric one $Ba_{0.8}Hf_{12}As_{17.7}$, a first approximation of the distribution of electrons via the Zintl scheme (metal atoms transferring their valence electrons to the nonmetal atoms) dictates that the As atoms cannot attain an octet without forming additional homoatomic bonds. For instance, the idealized formulation $(Ba^{2+})[(Hf^{4+})_{12}(As^{2.1-})_{24}]$ implies that, on average, each As atom has only 7.1

(30) $Cr_{12}P_7$: Chun, H. K.; Carpenter, G. B. *Acta Crystallogr., Sect. B: Struct. Crystallogr. Cryst. Chem.* **1979**, *35*, 30.
(31) Th_7S_{12}: Zachariasen, W. H. *Acta Crystallogr.* **1949**, *2*, 288.
(32) $Rh_{12}As_7$: Pivan, J.-Y.; Guérin, R.; Sergent, M. *J. Less-Common Met.* **1985**, *107*, 249.
(33) $Rh_{12}As_7$: Lambert-Andron, B.; Dhahri, E.; Chaudoüet, P.; Madar, R. *J. Less-Common Met.* **1985**, *108*, 353.
(34) $Ho_6Ni_{20}P_{13}$: Pivan, J.-Y.; Guérin, R.; Padiou, J.; Sergent, M. *J. Less-Common Met.* **1986**, *118*, 191.
(35) $Zr_6Ni_{20}P_{13}$: Guérin, R.; El Ghadraoui, E. H.; Pivan, J.-Y.; Padiou, J.; Sergent, M. *Mater. Res. Bull.* **1984**, *19*, 1257.
(36) $U_6Ni_{20}P_{13}$, $U_6Ni_{20}As_{13}$: Troc, R.; Kaczorowski, D.; Noël, H.; Le Bihan, T. *J. Alloys Compd.* **1992**, *184*, L27.
(37) $Tl_6Ag_{20-x}Se_{14-y}$: Klepp, K. O. *J. Less-Common Met.* **1987**, *128*, 131.
(38) $Ho_6Ni_{20}P_{13}$ ($P6_3/m$)[34] is essentially isotypic to $Zr_6Ni_{20}P_{13}$ ($P\bar{6}$).[35] We have chosen the former designation for the basis of comparison to "$BaHf_{12}As_{24}$", which also crystallizes in $P6_3/m$. The space group problem is discussed in: Jeitschko, W.; Jakubowski-Ripke, U. *Z. Kristallogr.* **1993**, *207*, 69.

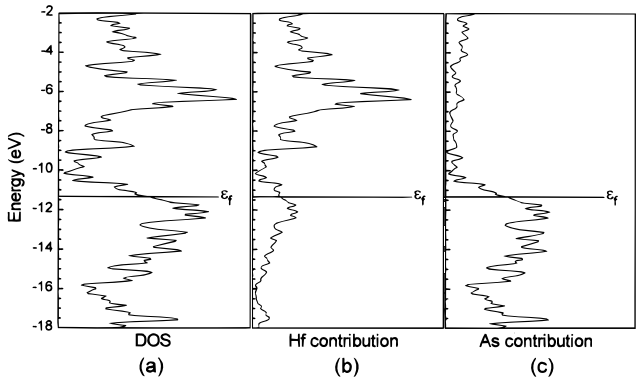

Figure 7. Density of states curve (and its Hf and As projections) for the $[Hf_{12}As_{24}]$ framework in idealized "$BaHf_{12}As_{24}$". The Fermi level ($\epsilon_f = -11.4$ eV) corresponding to substoichiometric $Ba_{0.8}Hf_{12}As_{17.7}$ is shown (assuming rigid band model).

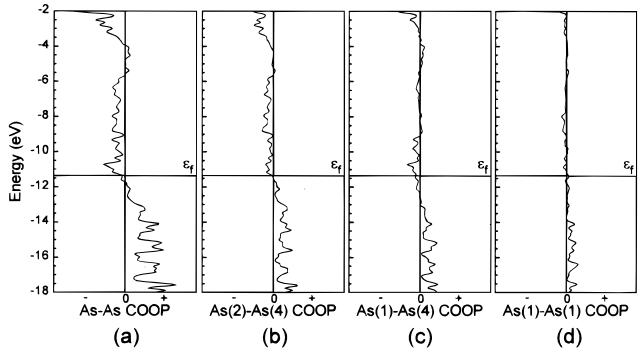

Figure 8. Crystal orbital overlap population curves for ((a) all; (b)−(d) specific) As−As contacts within the As ribbon of the $[Hf_{12}As_{24}]$ framework. The Fermi level corresponding to substoichiometric $Ba_{0.8}Hf_{12}As_{17.7}$ is shown.

valence electrons available to it, so that some As−As bonding must occur. For the observed nonstoichiometric composition and assuming As(3) to be As^{3-}, the more detailed formulation $(Ba^{2+})_{0.8}[(Hf^{4+})_{12}(As(3)^{3-})_6(As^{2.7-})_{11.7}]$ also implies that As is not fully reduced within the ribbons and that weak As−As bonding is present. This ionic extreme is not expected to be realistic, of course.

The band structure calculation on the ideal $[Hf_{12}As_{24}]$ framework confirms the presence of significant covalency in the Hf−As bonds. As shown in Figure 7, both Hf and As states have substantial contributions to the DOS in the region −16 to −10 eV. Equally important, the Hf and As bands are broad enough to overlap such that there is no energy gap. Assuming a rigid band model, the Fermi level in the actual compound (substoichiometric in As) falls in the valence band, consistent with the metallic behavior observed experimentally. Certainly, the presence of As vacancies will modify the details of orbital overlap in the true electronic structure, but limitations in the EHMO framework preclude a straightforward way of modeling vacancies. Particularly satisfying, nonetheless, is that even this simple band picture provides insight as to why As deficiencies occur in $Ba_{0.8}Hf_{12}As_{17.7}$. Figure 8 shows the COOP curves for the As−As contacts within the As ribbons in the structure. At the electron count corresponding to the observed stoichiometry, the Fermi level just separates the As−As bonding states from the As−As antibonding states; that is, the extent of As−As

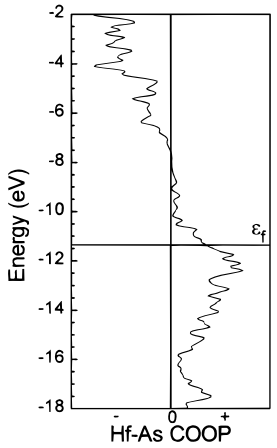

Figure 9. Crystal orbital overlap population curve for Hf−As contacts in the $[Hf_{12}As_{24}]$ framework. The Fermi level corresponding to $Ba_{0.8}Hf_{12}As_{17.7}$ is shown.

bonding is maximized at precisely this electron count. Within this ribbon (Figure 2), the average integrated As−As overlap population is 0.476, indicating fairly strong bonding interactions. The alternation of strong and weak As−As bonding (integrated overlap populations: As(2)−As(4) 0.553, As(4)−As(1) 0.389, As(1)−As(1) 0.499) is reminiscent of a similar pattern observed in the ribbons of Sb atoms in β−$ZrSb_2$.[39] The depopulation of the As−As antibonding states occurs at the expense of Hf−As bonding. Figure 9 shows the COOP curve for the Hf−As bonds in the structure. The Fermi level is lowered to a point below which depletion of strongly Hf−As bonding levels would no longer be compensated by any further gain in As−As bonding within the ribbons.

Overall, the band structure is in good agreement with the qualitative picture expected for a compound displaying homoatomic bonding of only the nonmetal component.[1] The overlap of As p states with Hf d states that can accept electron density back from the higher-lying As−As antibonding states is in part responsible for the metallic conduction.

There is an immense structural diversity displayed by the hexagonal structures built up from trigonal prisms centered by metal atoms. Generally these compounds are metal-rich, and metal−metal bonding is a predominant feature. The identification of $Ba_{0.8}Hf_{12}As_{17.7}$ is significant in that it implies the existence of an equally rich family of inversely related structures in which nonmetal−nonmetal bonding plays the important stabilizing role.

Acknowledgment. This work was supported by the Natural Sciences and Engineering Research Council of Canada and the University of Alberta. We are grateful to Dr. Robert McDonald (Faculty Service Officer, Structure Determination Laboratory) for the data collection and to Mr. Hong Wee Tan and Dr. John Beamish (Department of Physics) for assistance in the resistivity measurements.

Supporting Information Available: A listing of X-ray powder diffraction data (2 pages). One X-ray crystallographic file, in CIF format, is available. Ordering and access information is given on any current masthead page.

IC980545I

(39) Garcia, E.; Corbett, J. D. *J. Solid State Chem.* **1988**, *73*, 452.